Hot pixel classification of single-photon avalanche diode detector arrays using a log-normal statistical distribution

Hot pixel classification of single-photon avalanche diode detector arrays using a log-normal statistical distribution

P.W.R. Connolly✉, X. Ren, R.K. Henderson and G.S. Buller

CMOS single-photon avalanche diode (SPAD) detector arrays are commonly used in low-light imaging applications, and are known to suffer from certain defects which cause 'hot pixels'. These are detectors which exhibit a significantly larger than average dark count rate, adding noise to the data. Typically, data from these detectors are removed by post-processing or the detectors can, in some cases, be switched off prior to measurement. Users must define and identify these hot pixels, however there exists no consistent methodology of doing so. The authors present a self-consistent method of defining a hot pixel by fitting a log-normal distribution to a histogrammed dark-count map of the array. The approach has proven a robust method of classifying hot pixels in a number of different detector arrays, providing a threshold based on statistical analysis rather than human intuition. This definition provides a reliable and standardised figure of merit, facilitating a more accurate comparison between different single-photon detector arrays.

Introduction: The field of single-photon detection and imaging is a rapidly expanding area of research, with single-photon avalanche diode (SPAD) arrays becoming increasingly more widely used in areas such as fluorescence-lifetime imaging microscopy [1], 2D imaging [2], depth profiling [3, 4] and time-of-flight imaging [5]. As these detector arrays become more prevalent, methods of characterisation must be consistent across all formats of detector. A common defect in SPAD detector arrays is the occurrence of what is typically described as a 'hot pixel': one whose dark count rate (DCR) is significantly higher than the average of the array, and will present as a bright spot in any single-photon greyscale or intensity image [6–8], as shown in Fig. 1. The behaviour of these hot pixels has been shown to be largely attributable to mid-bandgap traps, causing the activation energy of the pixel to reduce substantially and therefore resulting in a lower breakdown voltage [9]. With a common bias across the detector array, this lower breakdown voltage results in much higher DCR in these particular pixels.

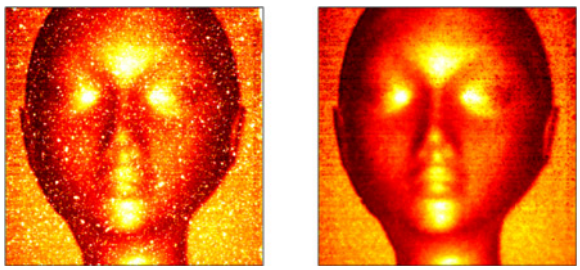

a *b*

Fig. 1 *Intensity recording of a polystyrene human head taken with a* 256 × 256 *Si-SPAD array*

a Intensity image affected by hot pixels
b Hot pixels have been identified and removed using our algorithm and filled in using a 3 × 3 median filter

While hot pixels may still contain useful data, in many applications it is often more practical to simply discard the pixel in question and reconstruct its content using information from the surrounding pixels. Due to optical cross-talk, a hot pixel may also affect surrounding pixels via photon emission from the hot pixel being absorbed by one of its neighbours, increasing the noise in these pixels [7, 10]. For these reasons it is critical to identify hot pixels which can either be removed in post-processing the image data or switched off prior to the measurement, where permitted by the device.

Hot pixel identification: There are different methods of identifying hot pixels, though generally one of two approaches is used to set a threshold, above which a pixel is considered 'hot'. Firstly, the threshold may be set as a simple multiple of the median value, i.e. $\mathcal{F} \times \mathcal{M}$, where $\mathcal{M}$ is the median value of the DCR and the factor chosen for $\mathcal{F}$ is user defined. As such, the factor chosen can vary drastically, with values used from as little as $\mathcal{F} = 2.5$ [11] to as much as $\mathcal{F} = 100$ [12]. This variation in $\mathcal{F}$ is due, in part, to the median value not necessarily being correlated to the width of the DCR distribution. Hence, a higher median DCR will require a lower multiplicative $\mathcal{F}$ factor. Alternatively, some authors have chosen to set an arbitrary threshold value to exclude the noisiest pixels [13, 14].

To exclude the same pixels each time, this threshold will need to be changed depending upon ambient temperature and bias voltage, as both will affect the DCR distribution. Neither of these approaches can be consistently applied with the same parameters to either multiple detectors, or multiple measurements using an individual detector under changing environmental or operating conditions. In order to devise a self-consistent methodology of defining and identifying hot pixels regardless of detector type, size of array, temperature or bias voltage, we examine the generation mechanisms of dark counts and the origin of hot pixels.

Dark counts occur primarily due to either thermal emission of electrons or band-to-band tunnelling, however afterpulsing and crosstalk will also contribute to DCR [9, 15]. The relative contribution of each mechanism varies greatly from chip to chip, and depends on the composite materials in use, the operating temperature, breakdown voltage, excess bias, doping concentrations, number of impurities and thickness of the depletion zone [15]. Therefore, the DCRs of individual SPAD detectors cannot be predicted by simple analytical formulae. Variation in the DCRs of similar pixels across an array are primarily affected by inhomogeneities in the pixels occurring during the manufacturing process. These inhomogeneities may include variations in doping concentrations, as well as differences in the number and nature of impurities and defects in the bulk material that can cause afterpulsing [9]. These variations may reasonably be assumed to occur randomly, and as such, the statistical deviation in DCR over an array can also be considered random. Mathematically, a given random variable would follow a Gaussian, or normal distribution, however the nature of dark count emission enforces a constraint that values cannot be negative and are generally close to zero. This results in an asymmetrical, positively skewed distribution. The case is therefore most accurately represented by a log-normal, or Galton distribution, which is applicable to random, positive variables which have a few very large values [16].

The log-normal distribution has previously been used to describe random variation in physical systems affected by statistically independent variables, including the effects of atmospheric turbulence on the distribution of detected single-photon events [17, 18], and photo-emission from gamma ray bursts [19, 20]. To define a hot pixel therefore, we propose fitting a log-normal probability density function (pdf), defined by (1), to the dark count data, x, of an array, the logarithm of which will therefore form a Gaussian distribution. This underlying Gaussian distribution can be described by its arithmetic mean, μ - from which the log-normal distribution's geometric mean is obtained by e^{μ} - and standard deviation, σ, such that the interval $\mu - 3\sigma \rightarrow \mu + 3\sigma$ contains 99.7% of the total Gaussian distribution. Using the three-sigma result therefore translates to an upper threshold of $e^{\mu+3\sigma}$ on the log-normally distributed data.

$$\frac{1}{\sigma x\sqrt{2\pi}}\exp\left(-\frac{(\ln(x)-\mu)^2}{2\sigma^2}\right) \quad (1)$$

With appropriate values taken for μ and σ, this pdf may therefore be used to describe the DCR distribution of any given detector array. Accordingly, setting the three-sigma analytical limit will include the vast majority of pixels which fall within the predicted log-normal distribution, while excluding those pixels whose behaviour exceeds these bounds, which we may now define as 'hot'.

Results: The log-normal probability density function (1) is fitted to the histogram of dark counts per pixel. Values for μ and σ are determined using a maximum likelihood estimation approach, whereby μ and σ^2 are estimated as the mean and variance, respectively, of the natural logarithm of data. To ensure an appropriate fit, the distribution is applied to data $< 5 \times \mathcal{M}$, however this does not set $5 \times \mathcal{M}$ as the limit of the distribution, which may continue beyond this value. In order to evaluate the effectiveness of the approach a cumulative dark count plot is used, where the aggregate counts are plotted versus the percentage of detectors in the array when arranged from the lowest to highest DCR. A successful outcome is achieved if the

three-sigma threshold occurs just before the cumulative dark count plot transitions from a shallow to steep gradient, indicating the point at which the dark count values of the pixels begin to rapidly increase. We successfully tested this method on eighteen CMOS SPAD arrays, of seven different varieties of detector array design from multiple manufacturers. In this Letter, we present the results of this technique applied to three different array types. Results are presented for an MF32 chip [21], a 32 × 32 Si CMOS SPAD array (Fig. 2*a*); the QuantiCam [22], a 192 × 128 Si CMOS SPAD array (Fig. 2*b*); and a 512 × 512 Si CMOS SPAD array [12] (Fig. 2*c*). In all three cases, this log-normal fitting approach applies the threshold immediately prior to the point at which the cumulative dark count distribution transitions to a higher gradient - the ideal point above which to classify a pixel as 'hot'.

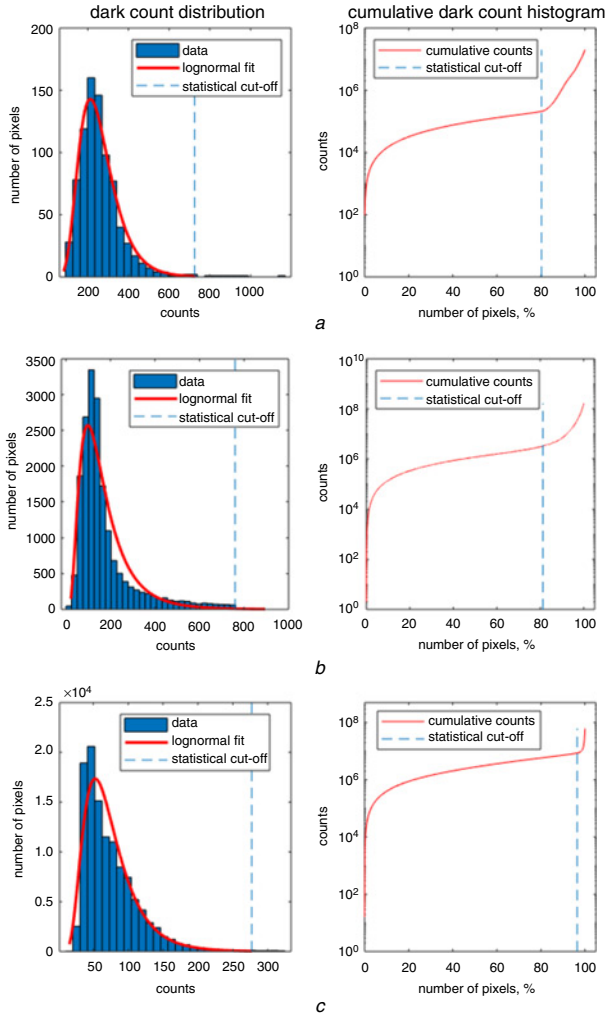

Fig. 2 *Dark count distributions (left) and cumulative dark count histograms (right) for*

a MF32, a 32 × 32 SPAD array
b Quanticam, a 192 × 128 SPAD array
c 256 × 472 pixels from a 512 × 512 SPAD array [12]

This technique, having been applied to four further SPAD detector arrays of different formats and fabrication methods, has covered a variety of well implant approaches, and CMOS technologies from 0.13 to 0.35 μm. This results in a wide range of DCR and hot pixel characteristics being examined, with similar results being observed in all cases.

Discussion and conclusion: We propose a statistical approach to defining and identifying hot pixels in a SPAD detector array through the fitting of a log-normal distribution and a threshold of three standard deviations from the mean of the underlying Gaussian distribution. This method is shown to be a robust approach to classifying hot pixels when applied to a variety of different chips of varying format, behaviour and fabrication technologies. Previous approaches consider each device on a case-by-case basis and rely on the judgement of the user to classify a hot pixel. This results in a lack of consistency and therefore relevance in using this figure of merit. This simple, adaptive approach may be applied without alteration to all arrays using a purely statistical methodology and requiring no user input. This algorithm could be used in varying environments, allowing a dynamic re-configuration of the hot pixel mask to optimise imaging performance under a variety of conditions.

Acknowledgments: The authors thank E. Charbon's group at École polytechnique fèdèrale de Lausanne for providing the dark count data from [12]. This work has been supported by the UK Engineering and Physical Sciences Research Council via projects EP/N003446/1 and EP/M01326X/1.

Submitted: *25 April 2019* E-first: *24 July 2019*
doi: 10.1049/el.2019.1427
One or more of the Figures in this Letter are available in colour online.

P.W.R. Connolly, X. Ren and G.S. Buller (*School of Engineering and Physical Sciences, Heriot-Watt University, Edinburgh EH14 4AS, UK*)

✉ E-mail: pc23@hw.ac.uk

R.K. Henderson (*School of Engineering, The University of Edinburgh, Edinburgh EH9 3JL, UK*)

References

1 Antolovic, I.M., Burri, S., Hoebe, R.A., *et al.*: 'Photon-counting arrays for time-resolved imaging', *Sensors*, 2016, **16**, p. 1005, doi: 10.3390/s16071005
2 Bronzi, D., Villa, F., Tisa, S., *et al.*: '100000 frames/s 64 × 32 single-photon detector array for 2-D imaging and 3-D ranging', *J. Sel. Top. Quantum Electron.*, 2014, **20**, pp. 354–363, doi: 10.1109/JSTQE.2014.2341562
3 Ren, X., Connolly, P.W.R., Halimi, A., *et al.*: 'High-resolution depth profiling using a range-gated Si CMOS SPAD quanta image sensor', *Opt. Express*, 2017, **26**, (5), pp. 5541–5557, doi: 10.1364/OE.26.005541
4 Shin, D., Xu, F., Venkatraman, D., *et al.*: 'Photon-efficient imaging with a single-photon camera', *Nat. Commun.*, 2016, **7**, p. 12046, doi: 10.1038/ncomms12046
5 Gersbach, M., Maruyama, Y., Trimananda, R., *et al.*: 'A time-resolved low-noise single-photon image sensor fabricated in deep-submicron CMOS technology', *J. Solid-State Circuits*, 2012, **47**, (6), pp. 1394–1407, doi: 10.1109/JSSC.2012.2188466
6 Gyongy, I., Davies, A., Dutton, N., *et al.*: 'Smart-aggregation imaging for single molecule localisation with SPAD cameras', *Sci. Rep.*, **6**, 2016, pp. 1–6, doi:10.1038/srep37349
7 Maruyama, Y., and Charbon, E.: 'A time-gated 128 × 128 CMOS SPAD array for on-chip fluorescence detection'. Proc. Int. Image Sensor Workshop, Hokkaido, Japan, June 2011, pp. 270–273
8 Villa, F., Bronzi, D., Bellisai, S., *et al.*: 'SPAD imagers for remote sensing at the single-photon level', *Proc. SPIE*, 2012, **8542**, pp. 1–6, doi: 10.1117/12.974532
9 Webster, E.A.G., and Henderson, R.K.: 'A TCAD and spectroscopy study of dark count mechanisms in single-photon avalanche diodes', *Trans. Electron Dev.*, 2013, **60**, (12), pp. 4014–4019, doi: 10.1109/TED.2013.2285163
10 Aull, B.F., Schuette, D.R., Young, D.J., *et al.*: 'A study of crosstalk in a 256 × 256 photon counting imager based on silicon Geiger-mode avalanche photodiodes', *Sens. J.*, 2015, **15**, (4), pp. 2123–2132, doi: 10.1109/JSEN.2014.2368456
11 Intermite, G., McCarthy, A., Warburton, R., *et al.*: 'Fill-factor improvement of Si CMOS single-photon avalanche diode detector arrays by integration of diffractive microlens arrays', *Opt. Express*, 2015, **23**, (26), pp. 33777–33791, doi: 10.1364/OE.23.033777
12 Ulku, A.C., Bruschini, C., Antolovic, I.M., *et al.*: 'A 512 × 512 SPAD image sensor with integrated gating for widefield FLIM', *J. Sel. Top. Quantum Electron.*, 2018, **25**, (1), p. 6801212, doi: 10.1109/JSTQE.2018.2867439
13 Nissinen, I., Nissinen, J., Keranen, P., *et al.*: 'A 16 × 256 SPAD line detector with a 50-ps, 3-bit, 256-channel time-to-digital converter for raman spectroscopy', *Sens. J.*, 2018, **18**, pp. 3789–3798, doi: 10.1109/JSEN.2018.2813531
14 Antolovic, I.M., Bruschini, C., and Charbon, E.: 'Dynamic range extension for photon counting arrays', *Opt. Exp.*, 2018, **26**, (17), pp. 22234–22248, doi: 10.1364/OE.26.022234

15 Palubiak, D.P., and Deen, M.J.: 'CMOS SPADs: design issues and research challenges for detectors, circuits, and arrays', *J. Sel. Top. Quantum Electron*, 2014, **20**, (6), p. 6000718, doi: 10.1109/JSTQE.2014.2344034
16 Forbes, C., Evans, M., Hastings, N., *et al.*: 'Statistical distributions' (John Wiley & Sons Inc., Hoboken, NJ, USA, 2011, 4th edn.), p. 131
17 Sjoqvist, L., Gronwall, C., Henriksson, M., *et al.*: 'Atmospheric turbulence effects in single-photon counting time-of-flight range profiling', *Proc. SPIE*, 2008, **7115**, pp. 1–12, doi: 10.1117/12.800241
18 Milonni, P.W., Carter, J.H., Peterson, C.G., *et al.*: 'Effects of propagation through atmospheric turbulence on photon statistics', *J. Opt. B, Quantum Semiclass. Opt.*, 2004, **6**, p. S742, doi: 10.1088/1464-4266/6/8/018
19 Li, H., and Fenimore, E.E.: 'Log-normal distributions in gamma-ray burst time histories', *Astrophys. J*, 1996, **469**, (2), p. L115, doi: 10.1086/310275
20 Kumar, P., and Zhang, B.: 'The physics of gamma-ray bursts and relativistic jets', *Phys. Rep.*, 2015, **561**, pp. 1–109, doi: 10.1016/j.physrep.2014.09.008
21 Richardson, J., Walker, R., Grant, L., *et al.*: 'A 32 × 3250 ps resolution 10 bit time to digital converter array in 130 nm CMOS for time correlated imaging'. Proc. of IEEE Conf. on Custom Integrated Circuits, San Jose, CA, USA, September 2009, pp. 77–80, doi: 10.1109/CICC.2009.5280890
22 Henderson, R.K., Johnston, N., Chen, H., *et al.*: 'A 192 × 128 time correlated single photon counting imager in 40 nm CMOS technology'. 44th European Solid-State Circuits Conf., Dresden, Germany, September 2018, doi: 10.1109/ESSCIRC.2018.8494330